MDPI

Article

Neutron-Enhanced Information on the Laboratory Characterization of Ancient Egyptian Leathers: Hydration and Preservation Status

Giovanni Romanelli [1], Carla Andreani [1], Enrico Ferraris [2], Christian Greco [2], Salima Ikram [3], Silvia Licoccia [4], Giuseppe Paladini [5], Stewart F. Parker [6], Enrico Preziosi [1,*], Roberto Senesi [1], Lucy Skinner [7], André J. Veldmeijer [3], Valentina Venuti [5] and Valentina Turina [2]

[1] Physics Department and NAST Centre, Università degli Studi di Roma "Tor Vergata", Via della Ricerca Scientifica 1, 00133 Rome, Italy
[2] Museo Egizio di Torino, Via Accademia delle Scienze 6, 10123 Turin, Italy
[3] Department of Sociology, Egyptology and Anthropology, The American University in Cairo, New Cairo 11835, Egypt
[4] Chemical Science and Technologies Department and NAST Centre, Università degli Studi di Roma "Tor Vergata", Via della Ricerca Scientifica 1, 00133 Rome, Italy
[5] Department of Mathematical and Computer Sciences, Physical Sciences and Earth Sciences (MIFT), University of Messina, Viale Ferdinando Stagno D'Alcontres 31, 98166 Messina, Italy
[6] ISIS Facility, STFC Rutherford Appleton Laboratory, Chilton, Didcot, Oxfordshire OX11 0QX, UK
[7] British Museum and the Institute of Creative Leather Technologies, University of Northampton, University Drive, Northampton NN1 5PH, UK
* Correspondence: enrico.preziosi@uniroma2.it

Abstract: The Museo Egizio's collection contains 200 precious and unique leather artifacts belonging to different historical periods. The materials used during the tanning and curing procedures affect the chemical and elemental composition of the surface of the samples as well as their preservation status, specifically through the hydration level within the bulk. Here we provide an experimental characterization of a series of samples from Museo Egizio that document an extensive denaturation phenomenon (gelatinization), by combining non-destructive techniques including surface probes (X-ray fluorescence, Raman scattering, and scanning electron microscopy enhanced by X-ray energy spectroscopy) and neutron-based bulk techniques (inelastic and deep-inelastic neutron scattering). Results show partial dehydration of the samples in the bulk, affecting the morphology of their surface, the presence of potassium alum, and iron oxides, as well as phosphates and hydroxides related to the tanning and curing procedures. Finally, we briefly discuss the need for a versatile and adaptable software package that is capable of combining quantitative analyses with complementary techniques including morphological, elemental, and chemical composition.

Keywords: cultural heritage; Egyptian leather; vibrational spectroscopy; Deep Inelastic Neutron Scattering; Scanning Electron Microscopy; elemental analysis

1. Introduction

The collection of Museo Egizio (Turin, Italy) [1] includes 200 leather objects of which approximately 10 exhibit extensive gelatinization. These leather objects were recovered throughout Egypt by various archaeological missions and are dated to different historical periods of Egypt, including the Old and New Kingdom, Roman, and Byzantine eras, thus ranging in date from ca. 2700 BC-AD 600. Leather is an organic material and therefore prone to various forms of deterioration. Through condition monitoring of the collection, different forms of degradation have been identified, suggesting a correspondence between their date and the type of deterioration. Moreover, the differences in degradation

may partially be the result of the manufacturing process and, specifically, of the substances with which the skins were treated. Examples include a sandal (Inv. N° S. 08640) from Kha's funeral equipment (around 1400 B.C.) [2]which is fragmentary and completely "gelatinized"(Figure 1).

(**a**)   (**b**)

Figure 1. Leather artifacts Inv. N° S. 08640: (**a**) Fragmentary and (**b**) completely gelatinized.

Ancient leather presents a heterogeneous composition of organic biomolecules—primarily fibrous proteins and lipids that exhibit reactivity as a function of the type of environmental exposure. Effective techniques for preservation remain challenging as some aspects of its chemical composition, degradation, and effectiveness of conservation treatments are yet to be fully understood [3]. Of particular concern for the collection at Museo Egizio is that skin processing methods (including any coloring treatments) and conservation treatments at the time of excavation, as well as the substances originally used to turn the material into leather, remain unknown. Three types of skin processes are mentioned in the literature: Vegetable tanning, which was likely not introduced until the Roman period; oil curing, also referred to as lipid tanning or leathering with oil and fat, which was the most used technique in pharaonic Egypt; and possibly alum and mineral treatments, although their use is uncertain [4–6].

Treatment-dependent damages to the artifacts are likely linked to the interaction between the materials used in the treatment and the collagen [7], the most important fibrous protein, constituting a wide variety of connective tissues in animals. The structure of collagen has been investigated extensively by electron microscopy and diffraction techniques using X-rays and neutrons [8–10]. From the mid-1970s, experimental and theoretical work on collagen was devoted to further the study of the dynamics of globular proteins [11] as motivated by the belief that much structural knowledge based on diffraction data needed to be complemented by the time domain to fully understand their functional properties.

In this work, we provide a broad characterization of a series of leather artifacts from the New Kingdom of ancient Egypt (1425-1353 B.C.) using a variety of surface and bulk techniques to quantify the hydration status of collagen. We also attempt to relate it to the methods and materials used during their tanning procedure. In particular, we performed experiments using X-ray Fluorescence (XRF), Raman spectroscopy, and Inelastic (INS) and Deep Inelastic Neutron Scattering (DINS) at the ISIS Neutron and Muon Source [12] complemented with Scanning Electron Microscopy (SEM) measurements. These techniques provide complementary information, allowing the study of a given sample from both the elemental and chemical standpoints. While XRF, Raman spectroscopy, and SEM instrumentation are available in laboratories of many research centers, neutron spectroscopies—optimal for studying the degree of hydration of the samples in the bulk—are only available at large-scale facilities such as ISIS. Therefore, the present investigation provides a worked example of how neutron-based techniques provide enhanced information to

complement that from table-top instrumentation, so as to understand and facilitate the preservation of Cultural Heritage artifacts.

2. Materials and Methods

A brief description of the samples is provided in Table 1. For all the experiments performed, the samples were measured as received without additional chemical or physical preparation.

Table 1. Reference number, mass, and description of the samples from Museo Egizio (Turin, Italy) used in the present study.

Sample Reference Number	Mass [mg]	Description
S1/S. 08640	403	Fragment from leather sandal, New Kingdom, XVIII Dynasty; Amenhotep II, Thutmose IV, Amenhotep III (1425-1353 B.C.)
S2/S. 14044	117	Fragment from leather sandal, Old Kingdom, V Dynasty (2435-2306 B.C.)
S3/S. 08369	264	Fragment from leather bag, New Kingdom, XVIII Dynasty, Amenhotep II, Thutmose IV, Amenhotep III (1425-1353 B.C.)
S4/S. 08507	30	Fragment from leather stool, New Kingdom, XVIII Dynasty, Amenhotep II, Thutmose IV, Amenhotep III (1425-1353 B.C.)
S5/S. 05150	8	Fragment from leather sandal, Late Period (722-332 B.C.)

XRF measurements were collected with a portable "Alpha 4000" analyzer (Innov-X system) that allowed the detection of various chemical elements with an atomic number (Z) between phosphorus (Z = 15) and lead (Z = 82). The apparatus was equipped with a Ta anode, X-ray tube, excitation source, and a high-resolution Si PIN diode detector (FWHM < 220 eV at 5.95 keV for Mn Kα line) characterized by an active area of 170 mm^2. The instrument was operated in "soil" mode, and two sequential tests were carried out on each sample. This procedure made the detection of elements possible from levels of ppm (parts per million). The working conditions were 40 kV and 7 µA for the first run (60 s collection time) and 15 kV and 5 µA for the second one (60 s collection time), for a total collection time of 120 s. A Hewlett-Packard iPAQ Pocket PC was employed to manage the instrument and as data storage. The calibration was performed by means of soil LEAP (Light Element Analysis Program) II and verified using alloy-certified reference materials produced by Analytical Reference Materials International. When detected, peaks at ~8.15 keV and ~9.34 keV have to be ascribed to Lα and Lβ transitions of the Ta anode.

Raman spectra were collected by means of a portable 'BTR 111 Mini-RamTM' (B&W Tek, USA) spectrometer. The instrument operated with a 785 nm excitation wavelength (diode laser), a 280 mW maximum laser power at the excitation port, and a thermoelectric cooled charge-coupled device (CCD) detector. The best signal-to-noise ratio in the minimum integration time was achieved by continuous adjustment of the laser output power. The spot size was 85 µm at a working distance of 5.90 mm. For our measurements, the maximum power of the samples was ~15 mW. All spectra were recorded in the 62-3153 cm^{-1} wavenumber range, with a resolution of 8 cm^{-1} and an acquisition time of 40 s, adding several scans for each spectrum to improve the signal-to-noise ratio. To ensure optimal instrument performance, a calibration procedure before each measurement was undertaken using the peak at 520.6 cm^{-1} of a silicon chip. The identification of the peaks was accomplished by comparing the measured spectra with data from databases and the literature [13,14].

Inelastic Neutron Scattering (INS) experiments were performed at the TOSCA spectrometer [15,16] at the ISIS Neutron and Muon Source (UK). TOSCA is an inverted-geometry spectrometer with final neutron energy fixed at ca. 3.5 meV. Spectra from both forward and backward scattering banks were used, positioned at ca. 42.5 and 137.8 degrees, respectively. Samples were wrapped in aluminium foil, inserted into the instrument's closed cycle refrigerator (CCR), and cooled in a He atmosphere (20 mBar) to 20 K, so as to maximize the instrument resolution by decreasing the Debye–Waller factor [17]. Measurement times ranged from 2 h for sample S1 to 12 h for sample S5, to collect comparable statistics given the much lower mass of the latter. Background measurements of the Al foil wrapping in the empty CCR were also collected for data reduction and analysis.

Deep Inelastic Neutron Scattering (DINS) measurements were performed with the VESUVIO spectrometer at ISIS [18–21]. VESUVIO is an indirect geometry spectrometer where the final neutron energy is fixed to ca. 4.9 eV by means of the lower-energy nuclear resonance in 197Au. Samples were measured at room temperature within the instrument tank in the same Al wrapping as the INS experiments on TOSCA and were run for similar acquisition times. Spectra were collected with the forward-scattering yttrium-aluminium-perovskite detectors [22] and the hydrogen neutron Compton profile was analyzed following the procedure described in Ref. [23,24]. The calibration of the concentration of hydrogen in the investigated samples from counts of mmol/100 mg was achieved by the measurement of a standard low-density polyethylene sample of dimensions 2 cm × 2 cm × 0.5 mm, with a known number of moles of hydrogen. The integrated signal from this reference sample was corrected by a factor of 0.83 due to self-shielding.

Scanning Electron Microscopy (SEM) measurements were performed at the ISIS@MACH ITALIA Research Infrastructure at the University of Rome "Tor Vergata" using a Tescan Vega (4th Series) with a GMU chamber. Back-scattering electron (BSE) and secondary electron (SE) images were collected in high-vacuum and environmental (7–20 Pa, with the Gaseous Secondary Electron Detector, GSD) conditions. To prevent sample contamination, the samples were examined without a conducting coating. A relatively low-current beam setup was used to avoid charging effects with an accelerating voltage of 5–20 kV. Energy Dispersive X-ray Spectroscopy (EDX) analyses were also performed at 20 keV accelerating voltage with the Xplore 30 EDS detector equipped in the SEM. SEM measurements were performed in low-vacuum conditions, to avoid charge effects of the sample without using a coating material (e.g., gold) on it, as well as to reduce the degassing and dehydration of the sample.

3. Results

3.1. XRF Analysis

XRF analyses were carried out on the front side and the corresponding leather substrate (back). The obtained elemental composition is reported in Table 2, whereas some representative XRF spectra, collected on the front and back sides of samples S1 and S4, respectively, are displayed in Figure 2.

Table 2. List of elements detected using XRF in the investigated samples, in order of abundance. Minor and trace elements are reported in parentheses.

Sample	Side	Elements
S1/08640	Front	Ca, Cl, S, K, Fe, Ti, (Ba, Sr, As, Br, Zr)
	Back	Ca, Cl, K, Ti, Fe, (Ba, Mn, Zr, Sr, Mo, Br)
S2/14044	Front	Ca, Cl, Ti, Fe, K, (Ba, Mn, Mo, Zr, Sr, Br, Rb)
	Back	Ca, Cl, S, Fe, K, Ti, (Ba, Mn, Cu, Mo, Zr, Sr, Br, Rb)
S3/08369	Front	Ca, Fe, K, S, Cl, Ti, (Cu, Mn, Ba, Sr, Pb, Zr, Zn, Mo, As, Br, Rb)

	Back	Ca, Fe, K, S, Cl, Ti, (Cu, Mn, Ba, Sr, Pb, Zr, Zn, Mo, As, Br, Rb)
S4/08507	Front	Ca, Ti, Cl, Ba, Fe, (Mo, Sr, Zr, Rb, Br)
	Back	Ca, Cl, Ti, K, Fe, (Ba, Sr, Mn, Mo, Zr, Br, Rb)
S5/05150	Front	Ca, Fe, Cl, K, Ti, (Ba, Mn, Sr, Mo, Zr, Br, Rb)
	Back	Ca, Cl, Ti, Fe, K, (Ba, Mn, Sr, Mo, Zr, Br, Rb)
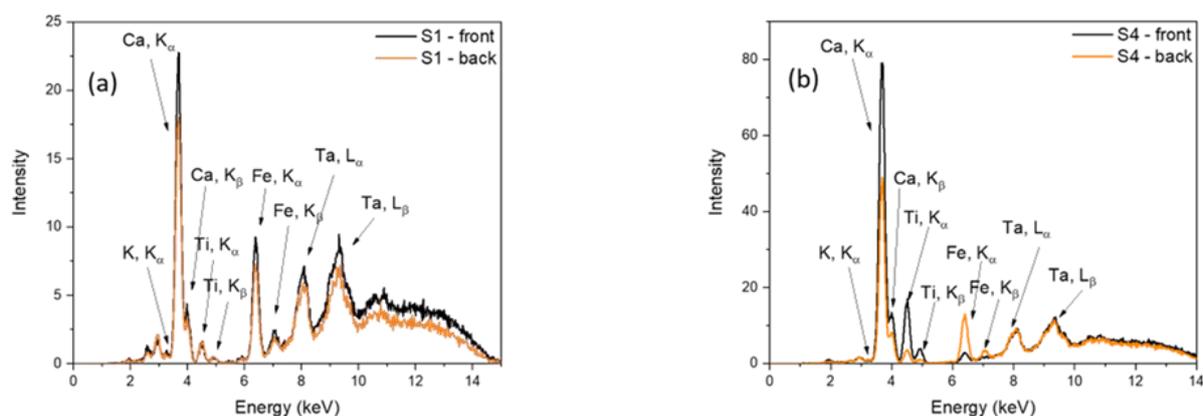
Figure 2. Representative XRF spectra, in the 0–14 keV range, collected on the front and back sides of samples S1 (**a**) and S4 (**b**).

All the investigated samples revealed the presence of Fe, K, and a large amount of Ca (see Table 2). The latter could be related to the depilation procedure during the pre-tanning process using calcium hydroxide (lime) [25], although it is unlikely that lime was used in Egypt for depilation before the 1st millennium AD. On the other hand, the presence of Fe could be easily ascribed to the use of impure potassium alum ($KAl(SO_4)_2$) in the tanning process, which contains large quantities of iron sulfate. Alum may have been used as a fixative to attach red madder dye to the leather surface (it is used as a mordant in dyes and to precipitate dyes in lake pigments). Furthermore, potassium alum obtained from natural alunite ($KAl_3(SO_4)_2(OH)_6$) through toasting, cleaning with lye, and crystallization can display a brownish color due to the presence of Fe_2O_3. Taking into account the aforementioned considerations, the presence of iron could likely be linked to the tanning procedure itself. It is worth noting that iron oxides are also contained in raw animal hides [26].

For all the investigated fragments, a comparison between the XRF spectra collected on the front and back sides evidence variations that testify to a slightly different elemental composition. In detail, passing from the back to the front side, an increased amount of Ca, along with a reduction in the amount of Fe, can be clearly recognized. Although there is no evidence of black colorants on the leather samples, the higher concentration of Ca could be due to the presence of an organic pigment brushed onto the topmost layer of the leather, such as bone black ($Ca_3(PO_4)_2 + C + MgSO_4$), whose key-element cannot be directly identified by XRF due to the low atomic number [25]. Other elements, such as Cl and Ti, could partly come from the raw hide or also be due to the leather processing technique. Furthermore, the presence of Sr may be correlated with the high intensities observed for Ca. In fact, since these elements possess remarkable chemical similarity, Sr atoms can replace Ca atoms in the crystal lattices of several substances [27]. Finally, when detected, traces of Cu could be related to degradation phenomena caused by copper chlorides, e.g., $Cu(OH)_2Cu(OH)Cl$ [28]. In this respect, it is worth noting that the green colorant on pharaonic period leather is a copper-based organo-metallic colorant (carboxylate green), and this could be related to the detection of copper.

3.2. Raman Spectroscopy Analysis

The molecular characterization of the leather fragments was first assessed through Raman spectroscopy. Comparable Raman spectra were obtained, as far as both front and back sides are concerned, for all the investigated samples, suggesting a similar molecular composition. Figure 3 reports two representative Raman spectra, in the 400–2500 cm^{-1} wavenumber region, collected on the front and back sides of sample S2, as an example. The Raman profile of both sides reveals the presence of iron oxides and hydroxides on the surface, through the detection of a band at ~610 cm^{-1}. The observation of a clearly visible band at ~940 cm^{-1} indicates the presence of phosphates, typically revealed in the presence of cellular material, which could suggest the application of proteinaceous compounds onto the top layer of the sample [29] and applies to the other samples investigated as well. The peak at ~1085 cm^{-1}, observed in the Raman profile of the back side only, indicates the presence of carbonates within the material. One could speculate that calcium carbonate might be used in skin processing, possibly mixed in with fats in the lipid tanning, to help the fats enter the fiber structure of the skin and stop the fibers from sticking together as the leather dries. Additionally, carbonates are also commonly found in soil with clays. Finally, the detection of two large bands centered at ~1400 cm^{-1} and ~1600 cm^{-1}, assigned to the D (disorder) and G (graphitic) bands of amorphous carbon, can be ascribed to either the application of bone black as black pigment or to partial carbonization and/or degradation of the sample [30]. The second hypothesis is more likely because of the high pollution level of Turin's city center (due to its geographical location between the alps and the hills of the Piemonte), the traffic situation until the 1990s (main streets were placed around the Museo Egizio), and, finally, the common problems connected to the use of a historical building as a place for the storage and conservation of historical artefacts as is in the case of Museo Egizio, which is within a 17th-century building (without insulation barriers until the beginning of the 21st century). All these factors likely caused, or at least increased, the formation of layers of dirt on the surface of objects (pollution). Moreover, a wax layer likely used as a consolidant in the early 20th century may be present in the artworks. Considering the sticky layer of wax and the presence of gas lamps in the building, as well as the pollutants mentioned above, there may be also a soot layer adhering to the objects.
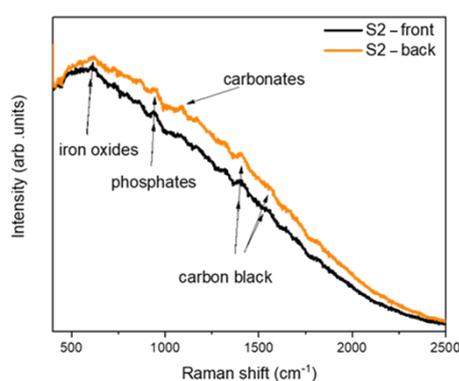

Figure 3. Representative Raman spectra, in the 400–2500 cm^{-1} region, recorded on the front and back sides of sample S2.

3.3. Neutron Scattering Analyses

3.3.1. Inelastic Neutron Scattering Analysis

To complement the information provided by XRF and Raman, which are mainly sensitive to medium- and heavy-atomic-weight elements, we performed neutron scattering experiments to determine the amount of water and hydrogen. Moreover, while the XRF and Raman results mentioned above are mainly related to the surface of the samples, neutron experiments provide information about the sample bulk, owing to the high penetration power of neutrons. First, samples were investigated using INS, vibrational spectroscopy allowing the detection of molecular and lattice vibrations involving hydrogen

[17,31], The collected spectrum from sample S1 is shown in Figure 4 together with the experimental background in the measurement. Spectra are composed of a series of broad features: Lattice modes are found below ca. 400 cm^{-1}; the strong peak at 250 cm^{-1} is the methyl torsion; librational modes from both tightly bound and interhelical water contribute to the region between 450 and 800 cm^{-1}; while modes associated with CH_2 and CH_3 bending are found in the region between 1200 and 1500 cm^{-1}. After normalization to the sample mass, the spectra from all the samples investigated were found to be overlapping, within experimental uncertainties.
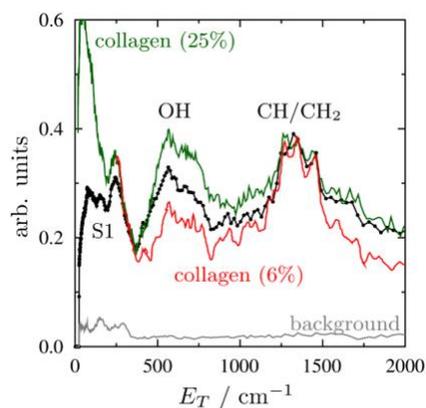
Figure 4. INS spectra of S1 and the experimental background from this work, compared to two reference spectra for collagen at hydration levels of 25% and 6% from Ref. [32].

Information about the level of hydration of the samples was achieved by comparing the intensity of the OH librational bands to two reference spectra of collagen hydrated at 6% and 25% from Ref. [32]. In order to analyze the amount of structural water, all the spectra were scaled so as to be overlapping in the energy region between 1200 and 1500 cm^{-1}, related to the CH_2 and CH_3 groups in the peptides' backbone in collagen. By analyzing the intensity of the signal in the OH librational region, the total hydration is estimated to be ca. 16%, i.e., 16 g of water per 100 g of dry collagen. This value is found to be constant, within uncertainties, amongst all the samples investigated.

3.3.2. Deep Inelastic Neutron Scattering Analysis

Additional information on the amount of hydrogen in the samples was obtained by DINS measurements [33]. DINS is a technique whereby the signal from each element is mass-separated in a series of Neutron Compton Profiles (NCPs). In particular, the hydrogen NCP is well-separated from those of higher mass elements, thus providing a quantitative way to assess the amount of hydrogen in bulk materials [34,35].

Figure 5a shows how the intensity of the DINS spectra in the time-of-flight domain scales with the mass of the sample. From the integrated signal of the spectra in the range of 200–300 μs, the amount of hydrogen was found to scale with mass according to the equation $\alpha(1 - exp(\beta m))$ [34], where α and β are free fitting parameters and m is the sample mass. The fitting procedure provided a concentration of 7.1 ± 0.5 mmol of H per 100 mg of sample. If one considers a typical collagen chain to be a polypeptide composed of glycine-proline-hydroxyproline [36], the amount of hydrogen in completely dry collagen would correspond to 8.1 mmol/100 mg of sample, while it would decrease to 7.8, 7.5, and 7.2 mmol/100 mg of sample, for collagen hydrated at 6%, 16%, and 25%, respectively. Despite the large error bar, due to the non-optimal shape of the samples for a DINS measurement, and the rough approximation of the composition of the leather samples, the value from this analysis is compatible with the results from the INS measurement.
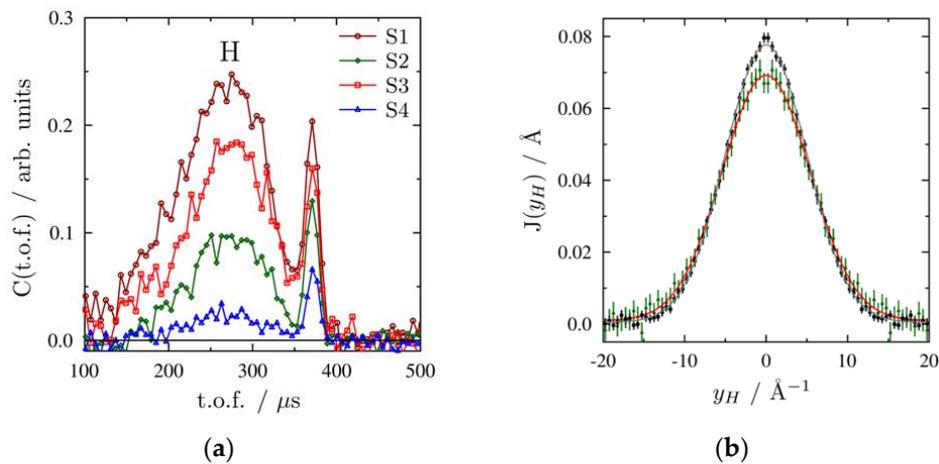
Figure 5. (**a**) DINS spectra of samples S1, S2, S3, and S4 in the time−of−flight domain. (**b**) Corrected H NCP in sample S1 (green error bar) together with its best fit (red line) and compared to the hydrogen NCP in polyethylene.

DINS allows a direct determination of the nuclear mean kinetic energy (NKE) of atoms in condensed matter from the analysis of NCPs [37–39]. Because of their quantum nature, the measured values of NKEs can be related to the local chemical potential and environment affecting nuclei and molecules in condensed matter. Therefore, DINS from sample S1 was analyzed to isolate the hydrogen NCP (see the right panel in Figure 5) providing an estimated value of the NKE of 174 ± 10 meV, higher than the value previously measured for bulk water at the same temperature, 146 ± 3 meV [40,41]. One should note that the measured value of the NKE in S1 could be affected by the irregular shape of the sample, as opposed to the reference value for room-temperature water, obtained in a canonical DINS experiment and suitable sample geometry. To quantify such effects, the same figure shows the comparison with the signal from a polyethylene sample, with a similar shape and dimensions as S1. We find that the NKE of polyethylene is 149 ± 6 meV, lower than the value found for sample S1, as one can appreciate from the narrower shape of the former compared to the latter in the right panel of Figure 5. An increased value of the NKE for a drier state of collagen is compatible with a scenario whereby the hydrogen mean kinetic energy arises mainly from the functional groups of the peptides. The higher value of the hydrogen NKE agrees with that found in dried DNA compared to the hydrated phase (see Ref. [42]).

3.4. Scanning Electron Microscopy Analysis

The amount of water in collagen largely affects its mechanical properties, as interstitial water is responsible for the network of interactions of nearby peptide chains. To obtain information on both the degradation state of our samples and the coating on their surface, we performed a series of SEM measurements. In vivo, collagen molecules adopt a quasi-hexagonal configuration in bundles referred to as fibrils [8]which are the first level of the collagen structure visible via SEM, and their appearance in the samples investigated is discussed below.

Figure 6a shows SEM images of samples S1 and S3 near fractures in the sample surface or where the surface seemed more degraded. For example, S3 showed a series of layers slowly detaching from each other. At the 10–20 μm scale, it is possible to observe the larger collagen bundles. Possibly due to the hydration level having decreased over the millennia, and consequently to a lower amount of interstitial water, which strengthens the material by linking adjacent peptides via hydrogen bonding, the material clearly shows a frayed surface.

Figure 6b shows the SEM images using back-scattering electrons (BSE) collected from sample S1 on the whole sample (A), magnifying the region delimited by the orange square

(B) and two details in the region within the yellow square (C and D). Sample S1 showed a broken surface with several fissures and cracks on the larger top and bottom surfaces, while the lateral surface was much smoother (see also Figure 1, right). The top surface presented a number of crystalline structures (Figure 6C,D) suggesting metal tanning of the leather, as already suggested by the XRF results above, or, considering that the fragment was part of a sandal, the inclusion of small stones as the shoe was worn. In addition, low magnification SEM images have been produced to obtain representative information from the overall sample. More specifically, images of the sample S1 were taken at approximately 90× magnification highlighting a rough surface (bright areas) on the micrometric scale, apparently due to a structured layer on the top of the leather surface. The cracking visible in panel B of Figure 6b is a clear consequence of the gelatinization phenomenon. From the BSE signal, this layer shows a homogeneous average atomic number across different areas of the sample.
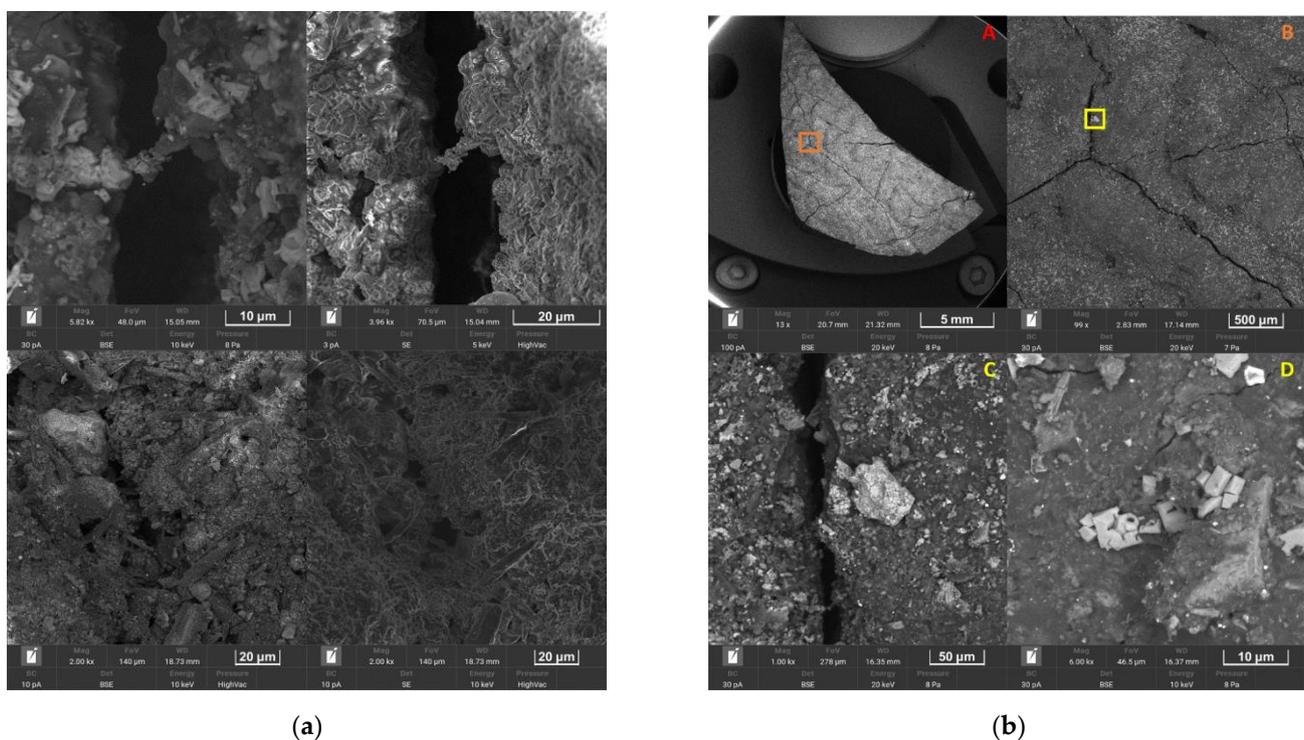

(**a**)   (**b**)

Figure 6. (**a**) SEM images of samples S1 (**top**) and S3 (**bottom**) obtained from back scattering (**left**) and secondary electrons (**right**). For each sample, the left and right panels correspond to the same region. (**b**) SEM images collected from sample S1 overall (**A**), maginification of the region delimited by the orange square (**B**) and two details in the region within the yellow square (**C**,**D**).

Energy Dispersive X-ray Spectroscopy Information

For a deeper understanding of the composition of the layer on the sample, and to complement the information from the XRF measurements, an EDX analysis was performed. This technique allows for the detection of the elements (down to Be) composing the sample in a point-by-point way. The results show different kinds of salts. First of all, NaCl covers most of the surface of the sample (see Figure 7), as well as salts composed of K, Mg, and Al. The point-by-point analysis shows, for example, that Ca salts can be found with different compositions such as $CaCO_3$, whose presence was already suggested above, as well as $CaSO_4$ and $CaCl_2$.
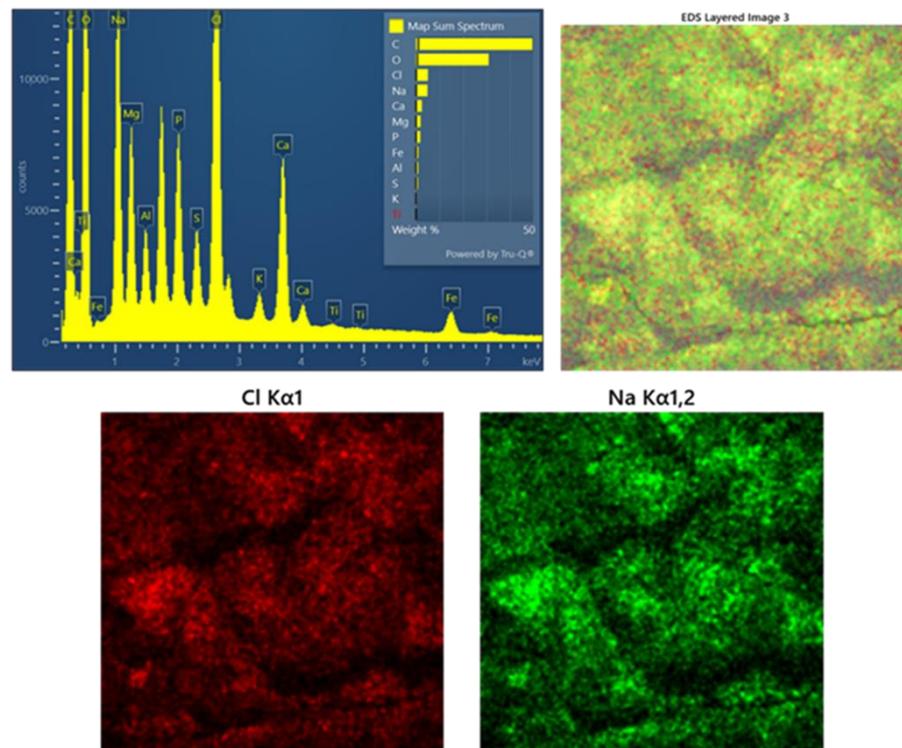
Figure 7. EDX spectrum obtained sample S1 (**top left**), related to the spatial distribution on a wide area of the sample of the different elements contributing to its composition (**top right**). The yellow color assigned to NaCl is due to the RGB superposition of the signals from Cl (in red, **bottom left**) and Na (in green, **bottom right**).

4. Discussion

A comprehensive understanding of the samples investigated in this work requires merging information from different, and complementary, experimental techniques. Figure 8 provides a pictorial view of how the techniques discussed above present a broad variety of information spanning the elemental or molecular nature of the signal, as well as a broad range of values of the atomic number Z, and therefore over the entire periodic table. In particular,

- Elemental composition: By merging XRF (more effective for elements with atomic number higher than 15) and EDS (effective for low atomic number elements), we provide a description of the substances used for tanning and possible contaminants during conservation. In addition, XRF provides information from the overall sample and from tens of microns below its surface while EDS gives punctual information from the first microns of the surface, allowing us to describe the very superficial layers of the sample. Moreover, DINS provides elemental information for Z = 1, which is difficult to access via photon-based techniques, helping to quantify the amount of water.
- Chemical composition: Through Raman spectroscopy, the chemical compositions of the tanning agents and pigments have been investigated (discovering carbonates and phosphates) and by INS, showing the amount of water in the bulk.
- Morphology characterization: Through SEM, the surface of the samples has been investigated on different length scales, highlighting the presence of salts, the composition of fibers, and the occurrence of cracking due to the low hydration and the gelatinization of collagen.
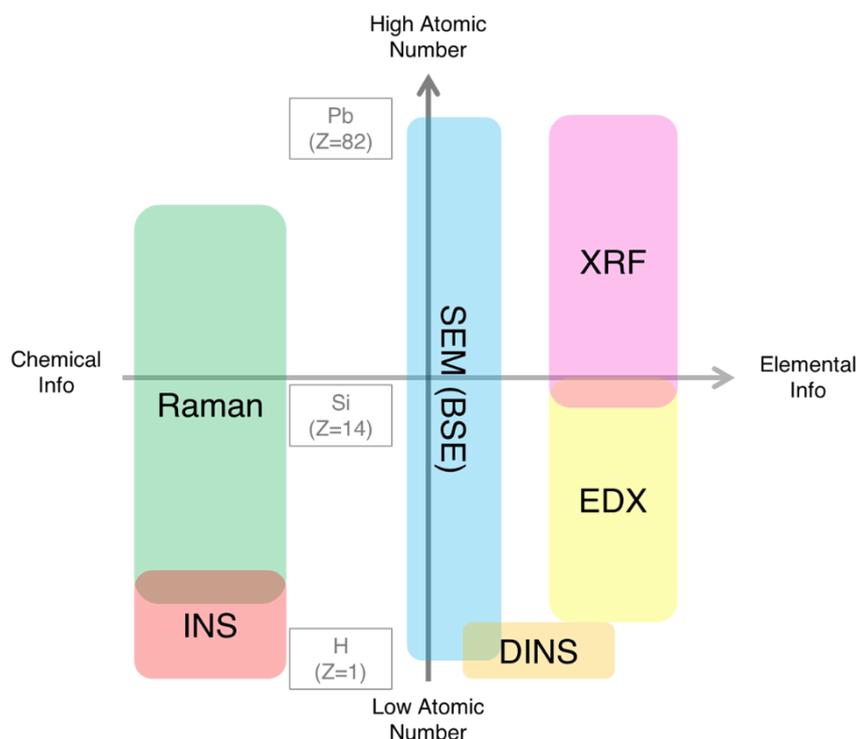
Figure 8. Schematic describing the kind of information available from each technique (chemical or elemental) and the dependence on the atomic number, highlighting the complementarity of the techniques involved in the analyses.

Despite the wealth of information provided by such a range of experimental techniques, it can be difficult to combine the results together to reconstruct a unified picture of the sample under investigation. At present, such a combined analysis would suffer from experimental differences, such as the volumes of sample probed (either on the surface or in the bulk) or the sensitivity of each technique. Information from these techniques can provide valuable details, allowing the reproducibility and comparison of experimental results, and should be collected and stored as metadata of the experiment.

To move beyond a qualitative description of the sample through its chemical and elemental compositions, one would need, in principle, a flexible tool (software) able to accept input information from very different techniques-some providing 1D spectra, 2D images, and multidimensional data—all based on different observables. However, as it is hard to imagine such software open to any technique, from the start, one should establish which techniques to consider, especially amongst the non-destructive ones suitable for Cultural Heritage objects [43,44], in order to obtain as general a picture as possible by using as limited a set of experimental techniques as possible. Through the discussion above, and by looking at Figure 8, we have confirmed the usefulness of table-top techniques and instrumentation—including XRF, Raman, and SEM-EDX—while demonstrating that an important range of complementary information can generally only be accessed using neutron-based techniques as well.

5. Conclusions

We have presented a multi-technique and multi-scale characterization of a series of leather artefacts from the New Kingdom of ancient Egypt (1425-1353 B.C.) using X-ray Fluorescence (XRF), Raman spectroscopy, Inelastic (INS) and Deep Inelastic Neutron Scattering (DINS), and Scanning Electron Microscopy (SEM). By combining the information gathered from both surface and bulk techniques and being sensitive to both the elemental and chemical composition of the samples, we inferred the hydration status of the sample

and some of the materials and techniques used for curing and tanning the leather artifacts. The amount of water, suggesting partial dehydration of the samples in the bulk, was linked to the morphology of their surface, showing partial degradation and gelatinization, with collagen layers slowly separating from each other. The analysis also showed the presence of potassium alum and iron oxides, possibly used for tanning and fixing, as well as phosphates and hydroxides, possibly related to oil curing of leather. Finally, traces of soot and dirt could be the result of the use of a wax layer as a consolidant at the beginning of the 20th century.

References

1. Museo Egizio. Available online: https://www.museoegizio.it/en/ (accessed on 15 June 2022).
2. Schiaparelli, E. *Relazione Sui Lavori della Missione Archeologica Italiana in Egitto (Anni 1903–1920): La Tomba Intatta Dell'architetto Cha, Nella Necropoli di Tebe*; R. Museo di Antichità: Torino, Italy, 1927.
3. Skinner, L.; Stacey, R.; Lama, A.; McGrath, K.; Cartwright, C.; Wills, B. Modified Methods for Species Identification of Archaeological Skin-based Objects: Dealing with Degradation and Improving Standards. In Proceedings of the 11th Interim Meeting of the ICOM-CC Leather and Related Materials Working Group (2021), Paris, France, 6–7 June 2019.
4. Van Driel-Murray, C. *Leatherwork and Skin Products. Ancient Egyptian Materials and Technology*; Cambridge University Press: Cambridge, UK, 2000; pp. 299–319.
5. Kite, M.; Thomson, R. (Eds.) *Conservation of Leather and Related Materials*; Routledge: London, UK, 2005.
6. Veldmeijer, A.J. Leather. In *Busy Lives at Amarna: Excavations in the Main City*; Kemp, B.J., Ed.; Grid 12 and the House of Ranefer, N49.18; Egypt Exploration Society/Amarna Trust: London, UK; Cambridge, UK, 2010; Volume II: The objects; pp. 205–212.
7. Larsen, R.; Sommer, D.V.P.; Axelsson, K.M.; Frank, S. Transformation of collagen into gelatine in historical leather and parchment caused by natural deterioration and moist treatment. In Proceedings of the ICOM-CC, Leather and Related Materials Working Group. Interim Meeting, Offenbach, Germany, 23–31 August 2012; Volume 31, pp. 61–68.
8. Miller, A. Collagen: The organic matrix of bone. *Philos. Trans. R. Soc. B: Biol. Sci.* **1984**, *304*, 455–477.
9. Fraser, R.; MacRae, T.; Miller, A. Molecular packing in type I collagen fibrils. *J. Mol. Biol.* **1987**, *193*, 115–125.
10. Wess, T.; Miller, A.; Bradshaw, J. Cross-linkage sites in type I collagen fibrils studied by neutron diffraction. *J. Mol. Biol.* **1990**, *213*, 1–5.
11. Karplus, M.; Petsko, G.A. Molecular dynamics simulations in biology. *Nature* **1990**, *347*, 631–639.
12. ISIS Neutron and Muon Source. Available online: https://www.isis.stfc.ac.uk/Pages/home.aspx (accessed on 15 June 2022).
13. Romanian Database of Raman Spectroscopy. Available online: http://rdrs.ro (accessed on 15 June 2022).
14. Lafuente, B.; Downs, R.T.; Yang, H.; Stone, N. The power of databases: The RRUFF project. In *Highlights in Mineralogical Crystallography*; De Gruyter: Berlin, Germany, 2005; pp. 1–30.

15. Parker, S.F.; Carlile, C.J.; Pike, T.; Tomkinson, J.; Newport, R.J.; Andreani, C.; Ricci, F.P.; Sacchetti, F.; Zoppi, M. TOSCA: A world class inelastic neutron spectrometer. *Phys. B Condens. Matter* **1997**, *241*, 154–156.

16. Pinna, R.S.; Zanetti, M.; Rudić, S.; Parker, S.F.; Armstrong, J.; Waller, S.P.; Zacek, D.; Smith, C.; Harrison, S.M.; Gorini, G.; et al. The TOSCA spectrometer at ISIS: The guide upgrade and beyond. *J. Phys. Conf. Ser.* **2018**, *1021*, 012029.

17. Fernandez-Alonso, F.; Price, D.L. *Neutron Scattering*; Academic Press: Cambridge, MA, USA, 2013.

18. Romanelli, G.; Krzystyniak, M.; Senesi, R.; Raspino, D.; Boxall, J.; Pooley, D.; Moorby, S.; Schooneveld, E.M.; Rhodes, N.J.; Andreani, C.; et al. Characterisation of the incident beam and current diffraction capabilities on the VESUVIO spectrometer. *Meas. Sci. Technol.* **2017**, *28*, 095501.

19. Andreani, C.; D'angelo, A.; Gorini, G.; Imberti, S.; Pietropaolo, A.; Rhodes, N.J.; Schooneveld, E.M.; Senesi, R.; Tardocchi, M. CdZnTe γ detector for deep inelastic neutron scattering on the VESUVIO spectrometer. *Appl. Phys. A* **2004**, *78*, 903–913.

20. Andreani, C.; Pietropaolo, A.; Senesi, R.; Gorini, G.; Tardocchi, M.; Bracco, A.; Rhodes, N.; Schooneveld, E. Electron-volt spectroscopy at a pulsed neutron source using a resonance detector technique. *Nucl. Instrum. Methods Phys. Res. Sect. A Accel. Spectrom. Detect. Assoc. Equip.* **2002**, *481*, 509–520.

21. Pietropaolo, A.; Andreani, C.; Rebai, M.; Giacomelli, L.; Gorini, G.; Cippo, E.P.; Tardocchi, M.; Fazzi, A.; Rinati, G.V.; Verona, C.; et al. Fission diamond detectors for fast-neutron ToF spectroscopy. *EPL (Europhys. Lett.)* **2011**, *94*, 62001.

22. Cippo, E.P.; Borella, A.; Gorini, G.; Kockelmann, W.; Moxon, M.; Postma, H.; Rhodes, N.J.; Schillebeeckx, P.; Schoonenveld, E.M.; Tardocchi, M.; et al. Imaging of cultural heritage objects using neutron resonances. *J. Anal. At. Spectrom.* **2011**, *26*, 992–999.

23. Andreani, C.; Pietropaolo, A.; Senesi, R.; Gorini, G.; Perelli-Cippo, E.; Tardocchi, M.; Rhodes, N.; Schooneveld, E.M. A resonant detector for high-energy inelastic neutron scattering experiments. *Appl. Phys. Lett.* **2004**, *85*, 5454.

24. Romanelli, G.; Hewer, B.; Krzystyniak, M.; Gigg, M.; Tolchenov, R.; Mukhopadhyay, S.; Fernandez-Alonso, F. Data analysis of neutron Compton scattering experiments using MANTID. *J. Phys. Conf. Ser.* **2018**, *1055*, 012016.

25. Mannina, L.; Lombardo, A. Diagnostic Analyses for the Study of Materials, Technique and State of Preservation of a Gilt and Painted Leather of the XVIII Century. *Procedia Chem.* **2013**, *8*, 202–211.

26. Rifkin, R. Assessing the Efficacy of Red Ochre as a Prehistoric Hide Tanning Ingredient. *J. Afr. Archaeol.* **2011**, *9*, 131–158.

27. Castro, L.N.C.; Calza, C.; Freitas, R.P.; Brancaglion, A.; Lopes, R.T. Analysis of ancient Egypt artifacts using X-ray fluorescence. In Proceedings of the IMEKO International Conference on Metrology for Archaeology and Cultural Heritage Torino, Italy, 19–21 October 2016.

28. Elnaggar, A.; Leona, M.; Nevin, A.; Heywood, A. The characterization of vegetable tannins and colouring agents in ancient Egyptian leather from the collection of the metropolitan museum of art. *Archaeometry* **2017**, *59*, 133–147.

29. D'Amico, S.; Venuti, V.; Colica, E.; Crupi, V.; Majolino, D.; Paladini, G.; Guido, S.; Mantella, G.; Zumbo, R. Scientific investigation of the Conversion of St Paul painting (Mdina, Malta). In Proceedings of the 2019 IMEKO TC4 International Conference on Metrology for Archaeology and Cultural Heritage, MetroArchaeo, Florence, Italy, 4–6 December 2019; pp. 330–334.

30. Venuti, V.; Fazzari, B.; Crupi, V.; Majolino, D.; Paladini, G.; Morabito, G.; Certo, G.; Lamberto, S.; Giacobbe, L. In situ diagnostic analysis of the XVIII century Madonna della Lettera panel painting (Messina, Italy). *Spectrochim. Acta A Mol. Biomol. Spectrosc.* **2019**, *228*, 117822.

31. Mitchell, P.C.H. *Vibrational Spectroscopy with Neutrons: With Applications in Chemistry, Biology, Materials Science and Catalysis*; World Scientific: Singapore, 2005; Volume 3.

32. Middendorf, H.; Hayward, R.; Parker, S.; Bradshaw, J.; Miller, A. Vibrational neutron spectroscopy of collagen and model polypeptides. *Biophys. J.* **1995**, *69*, 660–673.

33. Andreani, C.; Krzystyniak, M.; Romanelli, G.; Senesi, R.; Fernandez-Alonso, F. Electron-volt neutron spectroscopy: Beyond fundamental systems. *Adv. Phys.* **2017**, *66*, 1–73.

34. Krzystyniak, M.; Romanelli, G.; Fernandez-Alonso, F. Non-destructive quantitation of hydrogen via mass-resolved neutron spectroscopy. *Analyst* **2019**, *144*, 3936–3941.

35. Romanelli, G.; Liscio, A.; Senesi, R.; Zamboni, R.; Treossi, E.; Liscio, F.; Giambastiani, G.; Palermo, V.; Fernandez-Alonso, F.; Andreani, C. Soft confinement of water in graphene-oxide membranes. *Carbon* **2016**, *108*, 199–203.

36. Lodish, H.; Berk, A.; Zipursky, S.L.; Matsudaira, P.; Baltimore, D.; Darnell, J. Collagen: The Fibrous Protein of the Matrix. In *Molecular Cell Biology*, 4th ed.; WH Freeman and Company: New York, NY, USA, 2000.

37. Andreani, C.; Romanelli, G.; Senesi, R. Direct Measurements of Quantum Kinetic Energy Tensor in Stable and Metastable Water near the Triple Point: An Experimental Benchmark. *J. Phys. Chem. Lett.* **2016**, *7*, 2216–2220.

38. Senesi, R.; Romanelli, G.; Adams, M.; Andreani, C. Temperature dependence of the zero point kinetic energy in ice and water above room temperature. *Chem. Phys.* **2013**, *427*, 111–116.

39. Andreani, C.; Romanelli, G.; Senesi, R. A combined INS and DINS study of proton quantum dynamics of ice and water across the triple point and in the supercritical phase. *Chem. Phys.* **2013**, *427*, 106–110.

40. Andreani, C.; Senesi, R.; Krzystyniak, M.; Romanelli, G.; Fernandez-Alonso, F. Experimental studies of nuclear quantum effects in condensed matter: The case of water. *Riv. Nuovo Cim.* **2018**, *41*, 291–340.

41. Andreani, C.; Corsaro, C.; Mallamace, D.; Romanelli, G.; Senesi, R.; Mallamace, F. The onset of the tetrabonded structure in liquid water. *Sci. China Ser. G Phys. Mech. Astron.* **2019**, *62*, 107008.

42. Reiter, G.F.; Senesi, R.; Mayers, J. Changes in the Zero-Point Energy of the Protons as the Source of the Binding Energy of Water to A -Phase DNA. *Phys. Rev. Lett.* **2010**, *105*, 148101.

43. Costa, M.; Arruda, A.M.; Dias, L.; Barbosa, R.; Mirão, J.; Vandenabeele, P. The combined use of Raman and micro-X-ray diffraction analysis in the study of archaeological glass beads. *J. Raman Spectrosc.* **2018**, *50*, 250–261.
44. Portillo, H.; Zuluaga, M.C.; Ortega, L.A.; Alonso-Olazabal, A.; Murelaga, X.; Martinez-Salcedo, A. XRD, SEM/EDX and micro-Raman spectroscopy for mineralogical and chemical characterization of iron slags from the Roman archaeological site of Forua (Biscay, North Spain). *Microchem. J.* **2018**, *138*, 246–254.
45. Turina, V.; Ferraris, E.; Andreani, C.; Licoccia, S.; Romanelli, G.; Senesi, R.; Venuti, V. *Neutron Spectroscopy of Leather Artefacts from Museo Egizio (TOSCA), STFC ISIS Facility*; STFC ISIS Neutron and Muon Source: Oxford, UK, 2021. https://doi.org/10.5286/ISIS.E.RB2000211.
46. Turina, V.; Ferraris, E.; Andreani, C.; Licoccia, S.; Romanelli, G.; Senesi, R.; Venuti, V. *Neutron Spectroscopy of Leather Artefacts from Museo Egizio (VESUVIO), STFC ISIS Facility*; STFC ISIS Neutron and Muon Source: Oxford, UK, 2021. https://doi.org/10.5286/ISIS.E.RB2000210.